Three-dimensional electromagnetic and electrical inversions over the Antonio gold deposit in Peru

Michael S.G. McMillan, Douglas W. Oldenburg, UBC-Geophysical Inversion Facility, University of British Columbia*

SUMMARY

Electromagnetic (EM) and electrical geophysical datasets were acquired over the Antonio high sulfidation epithermal gold deposit in Northern Peru, and each dataset produced a three-dimensional resistivity inversion model which helped map geologic alteration. Time-domain airborne-EM and pole-dipole Induced-Polarization (IP) data were independently inverted, and compared to a Controlled-Source Audio-Frequency Magnetotellurics (CSAMT) 3D inversion. Absolute resistivity values were consistent across all three surveys and collectively they effectively outlined silicic alteration mapped from previous geologic work and drilling. For airborne-EM modeling, all 270 transmitter sources over the deposit region were included in the final inversion. This ability to model airborne-EM data in 3D with multiple transmitter sources demonstrates that large advancements have been made in recent years with inversion codes, data acquisition and processing. Using multiple datasets to accurately delineate silicic alteration is valuable for exploration purposes, as this highly resistive zone hosts much of the gold mineralization in the area.

INTRODUCTION

Electrical resistivity measures the degree to which a material opposes the flow of electric current, and can help distinguish rock types and alteration zones due to resistivity contrasts with background lithologies. Various geophysical methods attempt to recover the resistivity structure of the earth, and three procedures that will be discussed further are EM, DC/IP and CSAMT. This paper will focus on how time-domain EM, DC/IP and CSAMT 3D inversion models help establish a uniform explanation of the resistivity structure over the Antonio deposit, and how each model relates to surrounding geologic alteration. This work builds upon previous research by Oldenburg et al. (2004) which focused on 3D inversion results of CSAMT and DC/IP data in the area.

ANTONIO GEOLOGY BACKGROUND

The Antonio gold deposit is located within the larger Yanacocha high sulfidation epithermal system in mountainous Northern Peru. Newmont Mining Corporation owns the majority of this active mining and exploration project. Like many high sulfidation epithermal deposits, Antonio experienced pervasive hydrothermal alteration which texturally and chemically changed the nature of most preexisting rocks. The bulk of gold mineralization resides within alteration envelopes, and particularly within areas of silicic alteration such as massive silica, vuggy silica and granular silica. These quartz-rich areas of metasomatism are often found near faults where confined fluid flow occurred. Furthermore, the intersection of faults is especially prospective for gold mineralization where hydrothermal breccias broke through overlaying volcanic units (Pinto and Quispe, 2003). These structural traps within favorable pyroclastic lithologies, such as ignimbrite, beneath or proximal to flow dome complexes are typical geologic hosts to gold deposits in the region (Loayza and Reyes, 2010). Figure 1 shows a geology map of Antonio with common lithologies and structures marked. The primary extent of the deposit is circled in bold black.

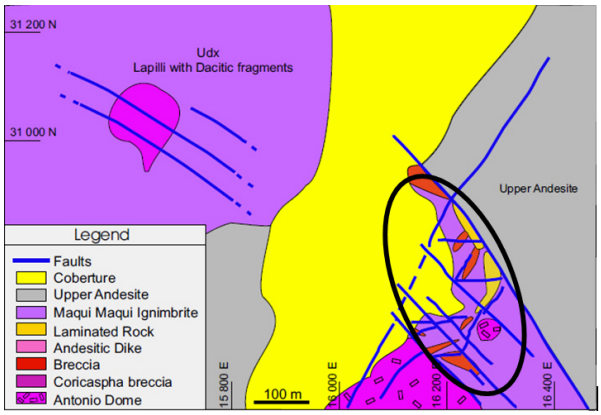

Figure 1: Antonio geology overview with deposit circled. Figure modified from (Oldenburg et al., 2004).

GEOPHYSICAL SURVEYS

Electromagnetic and electrical surveys were completed at Antonio with the intention of mapping silicic alteration. Host rocks which have undergone such alteration exhibit an elevated resistivity signature compared to surrounding units making them detectable through geophysical investigation. Since this alteration pattern is of prime exploration significance, defining its spatial extent in 3D both near-surface and at depth is clearly of interest for resource modeling and drill targeting. Firstly, a conventional time-domain pole-dipole DC/IP survey was conducted with five East-West oriented lines of variable lengths, spaced 150-200 meters apart using 50 meter spaced transmitter and receiver electrodes. DC/IP uses grounded electrodes to inject electric current into the subsurface while receiver electrodes throughout the survey grid measure electric potential differences. This survey was complimented with asynchronous scalar CSAMT data acquired by Quantec Geoscience including 11 East-West and 8 North-South lines. Station spacings were held constant at 50 meters and lines were separated by 150 meters. CSAMT uses a frequency-domain approach with grounded electrode sources situated well outside the survey region and receivers placed inside the area of interest which measure orthogonal pairs of electric and magnetic fields. Data at 13 frequencies were recorded ranging from 2Hz - 8192Hz.

DOI http://dx.doi.org/10.1190/segam2012-1316.1

In addition, airborne EM data were acquired with NEWTEM, a helicopter airborne time-domain EM system developed and internally operated by Newmont, (Eaton et al., 2002). This system achieved a peak current of 275 amps with a loop dipole moment of 80,000 Am^2. The secondary response was measured with time channels ranging from 10 microseconds to 6 milliseconds. NEWTEM was chosen as opposed to a ground EM survey because of its ability to rapidly collect data covering a large area of ground. Flights lines were flown in an East-West manner with data points separated by approximately 20 meters and adjacent lines spaced 200 meters apart. Antonio is one of many gold deposits in the Yanacocha region, and as such the NEWTEM data analyzed for this paper do not represent the entire airborne EM dataset, but a pertinent subsection of the survey area flown.

Figure 2 displays receiver locations for all three aforementioned geophysical surveys. It is worth noting that these techniques inherently differ in acquisition style, and on a project-to-project basis use contrasting station and line spacings. Consequently, data from these respective geophysical surveys may be unequally distributed throughout the survey area, but a common physical property is recovered, electrical resistivity. Therefore, the ultimate geophysical goal is for resistivity interpretations from multiple electromagnetic/electrical datasets to be consistent despite varying acquisition techniques and data concentrations.

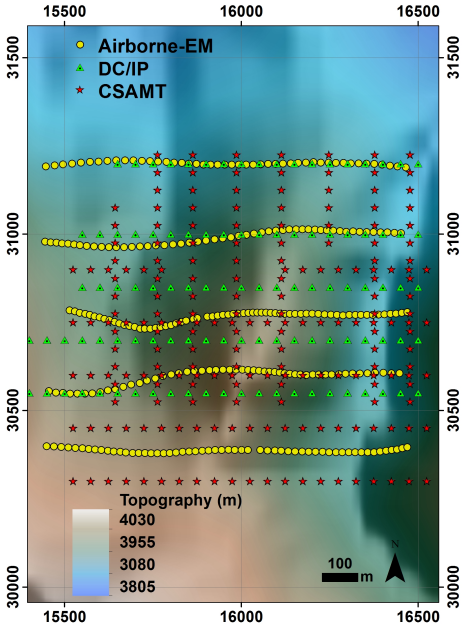

Figure 2: Antonio geophysical survey receiver locations overlaid on topography.

Time-domain airborne EM

Airborne time-domain data were inverted in 3D using 270 transmitter sources over the Antonio deposit using a multiple-source finite volume code, H3DTD, from the University of British Columbia (UBC) (Oldenburg et al., 2008). This Gauss-Newton based method intrinsically operates efficiently with many transmitters by using software called MUMPS (Amestoy et al., 2001) to compute a Cholesky decomposition of the forward modeling matrix. This involves discretely solving Maxwell's equations in both space and time:

$$\nabla \times E + \mu H_t = 0 \quad (1)$$

$$\nabla \times H - \sigma E - \varepsilon E_t = s_r(t) \quad (2)$$

subject to boundary conditions:

$$n \times H = 0 \quad (3)$$

and initial conditions:

$$E(x,y,z,t=0) = E_0 \quad (4)$$

$$H(x,y,z,t=0) = H_0 \quad (5)$$

E = electric field, H = magnetic field, μ = magnetic permeability, σ = electrical conductivity, ε = permittivity, s = source term, n = normal direction, x,y,z = Cartesian coordinates, t = time.

Once this large matrix has been factorized, solving the system for multiple sources becomes a relatively quick operation; however, this initial factorization is numerically intensive. To minimize computation time, H3DTD was run using multiple cores on a cluster computer at UBC. Prior to inversion, the original data were processed by Newmont, noisy time channels were discarded and errors of 15% plus a noise floor of 30 microvolts were assigned to the data. No additional constraints were applied apart from a suitable half-space resistivity value of 50 Ωm for the initial and reference model. As with other inversion codes, the mesh was padded with additional cells so that boundary conditions were satisfied. The cell sizes within the core region of the mesh were 50m x 50m x 25m in Easting, Northing and depth respectively. To ensure sufficient padding, two diffusion distances of the latest time channel separated the central mesh region from boundary cells. The diffusion distance for a particular time channel is given according to

$$d = \sqrt{\frac{2t}{\mu_0 \sigma}} \quad (6)$$

where μ_0 is the magnetic permeability of free space.

Figure 3(a) shows two images through the resulting airborne-EM 3D resistivity inversion model with the outer extent of silicic and silica-rich clay alteration shown as a dashed red polygon. Warmer colors represent higher resistivity values. To the left is a constant slice through the model at 3875 meters elevation which equates to an average depth below surface of approximately 50 meters. The image shows a high correlation with mapped silica alteration, as the center of the resistive anomaly coincides with the interior of the dashed polygon where intense vuggy and granular silica alteration has been

DOI http://dx.doi.org/10.1190/segam2012-1316.1

observed. A resistivity cross-section along line 30700N is displayed to the right in Figure 3(a) overlaid by a dashed outline of silica and silica-clay altered rock as defined by drilling. This image demonstrates that the airborne-EM 3D resistivity anomaly defines well the vertical and horizontal extent of silica alteration.

Further inversion improvements are being sought by using finer mesh cells along-line to take advantage of close data spacing. The large recovered EM resistivity anomaly has smooth edges with roughly homogeneous resistivity values in its interior. This is a characteristic appearance of a least-squares inversion algorithm result. Perhaps with tighter mesh cells, this indicated region can be further refined to glean additional spatial information from the data. Nevertheless, Figure 3(a) depicts encouraging results by demonstrating that even with a relatively coarse mesh, highly resistive alteration zones can be accurately mapped using 3D inversion models of time-domain airborne-EM.

DC/IP

DC/IP data were inverted for resistivity using DCIP3D (Li and Oldenburg, 2000) with assigned errors of 10% plus a noise floor of 1 mV. A 50 Ωm half-space discretized within a central 12.5m x 50m x 12.5m mesh was used as an initial and reference model. Figure 3(b) displays a constant elevation slice through the model at 3875m, and a cross-section along line 30700N. Worth noting is that a consistent resistivity color scale and alteration outline has been applied to all images in Figure 3. Overall the model produces a similar curved NNW trending resistivity feature as the airborne-EM survey, although only the western portion of the EM resistivity anomaly is coincidently mapped with a DC/IP resistivity high. This resistive feature overlaps with silica and clay-silica in the North-West domain of alteration, but elsewhere within the dashed outline there is poorer agreement. At the south-eastern extremity of alteration, the resistivity anomaly terminates well prior to the end of the silica zone. The cross-section appears similar, as the western portion of alteration is mapped well at depth whereas the eastern zone is mapped as mostly conductive.

EM and DC/IP resistivity anomalies do not have a perfect correlation especially in the eastern portion of the mapped alteration zone, but absolute resistivity values are comparable. This is important to recognize since EM and DC/IP surveys use inductive and galvanic sources respectively to excite the earth's subsurface. These two separate methods converging to an equivalent resistivity is evidence of recent improvements of geophysical inversion software and data processing. As for spatial inconsistencies, they could potentially be explained by sparse data coverage due to the presence of only five lines of DC/IP data. Alternatively, a slight coordinate shift could have occurred if an incorrect transformation was applied to convert data from one coordinate system to another. These possible explanations will be further investigated. Regardless of this outcome, the deposit area would be well suited for a "3D-style" densely spaced array of distributed IP data, such as Newmont's internally developed system: NewDAS (Eaton et al., 2010). The ensuing model could then be compared to its conventional IP counterpart.

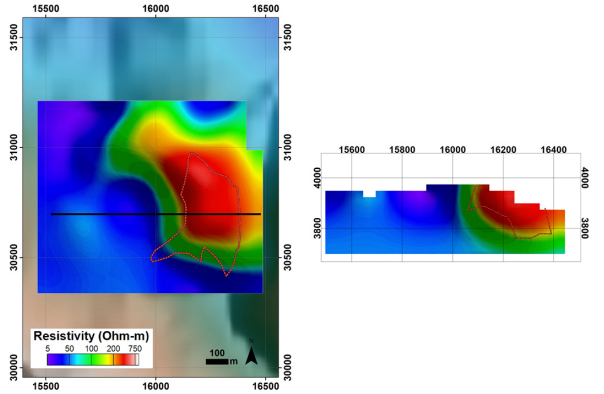

(a) Airborne-EM 3D Inversion. Silica and clay-silica alteration outlined in red. Left: Constant elevation, 3875m, resistivity plan map with line 30700N shown as a bold black line; Right: line 30700N resistivity cross-section.

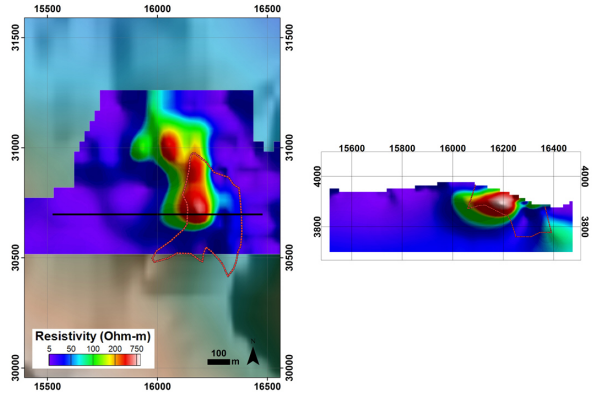

(b) DC/IP 3D Inversion. Silica and clay-silica alteration outlined in red. Left: Constant elevation, 3875m, resistivity plan map with line 30700N shown as a bold black line; Right: line 30700N resistivity cross-section.

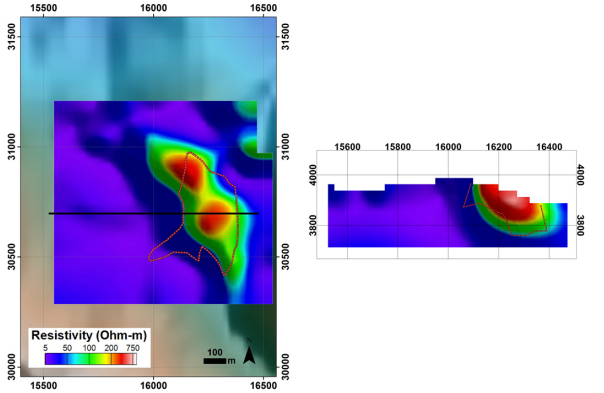

(c) CSAMT 3D Inversion. Silica and clay-silica alteration outlined in red. Left: Constant elevation, 3875m, resistivity plan map with line 30700N shown as a bold black line; Right: line 30700N resistivity cross-section.

Figure 3: 3D Resistivity inversion slices at 3875m elevation and cross-sections along 30700N. Constant elevation slices are overlaid on topography. All images use a consistent resistivity color scale.

DOI http://dx.doi.org/10.1190/segam2012-1316.1

CSAMT

A CSAMT inversion model outlined in Oldenburg et al. (2004) was used for comparison with EM and DC/IP results. EH3Dinv, a Gauss-Newton algorithm for frequency-domain EM data, as described in Haber et al. (2004), was used to invert the data to create this 3D volume. The original survey parameters consisted of a southern transmitter for East-West receiver lines and an eastern transmitter for North-South receiver lines. The transmitters were located many kilometers away from the core receiver area, which made establishing an appropriate mesh challenging. Large meshes made computation times impractical, and the solution chosen to counter this issue was to take a multi-step approach. To begin, a coarse mesh of 200 meter cells of constant 50 Ωm resistivity were forward modeled to establish expected electromagnetic fields at the edge of the core region. These fields were subsequently treated as boundary conditions for the ensuing inversion over the inner area which contained finer 50m x 50m x 25m cells. Amplitude and phase data from both transmitters were incorporated into the final inversion using frequencies of 4Hz and 64Hz with assigned errors of 10% plus a noise floor of 2 degrees.

Figure 3(c) displays a constant 3875m elevation slice and a cross-section through line 30700N within the Antonio portion of the 3D inversion model. The outline of silicic alteration matches well with the CSAMT resistivity anomaly in both plan and cross-section view. These results agree closely with those from airborne-EM. Resistivity values are also consistent with both airborne-EM and DC/IP models which suggests that these magnitudes are indeed appropriate for this area. An additional observation can be made: that the region shown by CSAMT to be highly resistive is divided into two distinct lobes as opposed to the one large zone depicted in the EM image. Whether this further refinement into two sections is geologically significant has yet to be determined, but will be a topic of future discussion. This resistivity separation can also be observed in the DC/IP result, despite the lobes being focused more to the North-West. In future work, the inversion program will be utilized to produce additional models that incorporate electric and magnetic fields from as many of the available 13 frequencies as possible. Particularly of interest will be whether or not significant changes occur to the observed resistivity pattern with these supplementary frequencies.

CONCLUSIONS

Three separate resistivity inversion models were analyzed over the Antonio high sulfidation epithermal deposit in Northern Peru. Time-domain airborne-EM (NEWTEM) and conventional pole-dipole IP data were inverted in 3D and compared with a 3D CSAMT inversion model. Consistent results were observed with regards to the spatial location and magnitude of resistive anomalies within EM and CSAMT models, whereas minor differences existed with the spatial extent of DC/IP derived resistors. Collectively the models accurately highlighted areas of resistive silica alteration known to host gold mineralization. When analyzed in further detail, the airborne-EM result was defined as a single resistive anomaly while DC/IP and CSAMT models showed the resistor as being partially separated into two lobes. The geologic significance of this disconnect is currently unknown, and will receive more attention in the coming months. Overall a high correlation to silicic alteration was shown by extracting elevation slices at 3875m through all three inversion models and comparing them to outlines of silica altered regions mapped from previous geologic work. Cross-sections through each 3D volume along East-West line 30700N showed that the depth extent of silica and silica-clay alteration was well defined by all three datasets in the western portion of the altered zone. In the eastern section, EM and CSAMT inversions produced resistors with a high agreement to silica alteration while the DC/IP result displayed a more conductive zone which has yet to be explained. Possible causes of this difference may be sparser data coverage of DC/IP data or issues stemming from coordinate transformations.

Altogether, this study has shown that 3D time-domain airborne-EM inversions provide valuable information at locations, such as Antonio, where resistivity contrasts are prominent and prospective for gold mineralization. The agreement in the recovered resistivities from the different field surveys is very encouraging and provides optimism that current data collection and analysis in 3D is reaching maturity. Notably, all resistivity models were produced using unconstrained inversions on relatively coarse meshes, meaning that further improvements can be achieved. Geologic constraints, such as petrophysical measurements from down-hole logging or drill-core, could be introduced as bounds or weights in future inversions. Constructing finer celled meshes for EM and CSAMT inversions would also be a logical progression. Other topics currently being looked into include incorporating more CSAMT frequencies, and attempting to remedy any inconsistencies in the DC/IP inversion results.

ACKNOWLEDGMENTS

The authors especially thank Rob Eso who, as a graduate student at UBC in 2003, carried out the first 3D inversions of the DC/IP and CSAMT data sets at Antonio, and showed the mutual agreement of the two inversions. A synoptic summary of those results was shown in Oldenburg et al. (2004), but unfortunately the detailed paper by Eso never materialized. We also thank Newmont Mining Corporation for permission to show this data, especially Perry Eaton for his support of university research and David Wynn for his adept programming skills. Further thanks goes to Elliot Holtham and all members of UBC-GIF for their support during this work.

DOI http://dx.doi.org/10.1190/segam2012-1316.1

http://dx.doi.org/10.1190/segam2012-1316.1

EDITED REFERENCES

Note: This reference list is a copy-edited version of the reference list submitted by the author. Reference lists for the 2012 SEG Technical Program Expanded Abstracts have been copy edited so that references provided with the online metadata for each paper will achieve a high degree of linking to cited sources that appear on the Web.

REFERENCES

Amestoy, R., I. D. J.-Y. L'Excellent, and J. Koster, 2001, A fully asynchronous multifrontal solver using distributed dynamic scheduling: Simax, **23**, 15–41.

Eaton, P., B. Anderson, I. Mackenzie, and D. Wynn, 2010, Newdas — The Newmont distributed IP data acquisition system: 80th Annual International Meeting, SEG, Expanded Abstracts, 1768–1771.

Eaton, P., B. Anderson, B. Nilsson, E. Lauritsen, S. Queen, and C. Barnett, 2002, Newtem — A novel time-domain helicopter electromagnetic system for resistivity mapping: 72nd Annual International Meeting, SEG, Expanded Abstracts, 1–4.

Haber, E., U. M. Ascher, and D. W. Oldenburg, 2004, Inversion of 3D electromagnetic data in frequency and time domain using an inexact all-at-once approach: Geophysics, **69**, 1216–1228.

Li, Y., and D. W. Oldenburg, 2000, 3D inversion of induced polarization data: Geophysics, **65**, 1931–1945.

Loayza, C., and J. Reyes, 2010, Geologic overview of the Yanacocha mining district Cajamarca, northern Peru: Presented at the SIMEXMIN10 — IV Brazilian Symposium of Mineral Exploration.

Oldenburg, D. W., E. Haber, and R. Shekhtman, 2008, Forward modeling and inversion of multisource tem data: 78th Annual International Meeting, SEG, Expanded Abstracts, 559–563.

Oldenburg, D. W., R. Shehktman, R. A. Eso, C. G. Farquharson, P. Eaton, B. Anderson, and B. Bolin, 2004, Closing the gap between research and practice in EM data interpretation: 74th Annual International Meeting, SEG, Expanded Abstracts, 1179–1182.

Pinto, R., and J. Quispe, 2003, Antonio project: Exploration and development final report: Minera Yanacocha Exploration Geology Department.